

Topological superconductivity in Rashba semiconductors without a Zeeman field

Panagiotis Kotetes*

*Institut für Theoretische Festkörperphysik and DFG-Center for Functional Nanostructures (CFN),
Karlsruhe Institute of Technology, 76128 Karlsruhe, Germany*

In this manuscript I present new hybrid devices based on multi-wire/channel Rashba semiconductors, which harbor Majorana fermions (MFs) *without* a Zeeman field. In contrast, magnetic fluxes, supercurrents or electric fields can be employed, yielding an enhanced device manipulability. The generic topological phase diagram for two-nanowire/channel systems exhibits features of quantum criticality and a rich interplay of phases with 0, 1 or 2 MFs per edge. The most prominent and experimentally feasible implementation relies on the already existing platforms of InAs-2DEG on top of a Josephson junction. Appropriate design of the latter device allows phases with 1 or 2 MFs, both detectable in zero-bias anomaly peaks with a single or double unit of conductance.

PACS numbers: 74.78.-w, 74.45.+c, 85.25.-j

I. INTRODUCTION

The perspective of topological quantum computing (TQC) [1] has motivated a plethora of proposals for engineering topological superconductors (TSCs), mostly relying on semiconductors with strong Rashba spin orbit coupling (SOC) [2–9]. Among them, a device involving a Rashba nanowire (NW) [3] lies in the spotlight of current research. The latter setup requires a sufficiently strong Zeeman field in order to enter the TSC phase with 1MF per edge. The first encouraging zero bias anomaly (ZBA) MF-findings have been already reported [10, 11], that however, remain under intense debate [12].

A promising route for resolving this controversy is to explore alternative TSC platforms which build upon the *same* materials used in these experiments but with the Zeeman field replaced by a supercurrent flow, an electric field or, as shown recently, by a SOC with time dependent orientation [8]. The latter ingredients appear less harmful for the bulk SC and possibly more versatile for TQC. For instance, existing TQC protocols rely on sufficiently strong antiparallel magnetic fields on a nanoscale level [13], which can be difficult to achieve in the lab. Instead, harboring MFs *all-electrically* can be advantageous for braiding and developing TSC circuits.

In this work, I propose a new type of artificial TSCs consisting of conventional SCs in proximity to *quasi-1d* semiconductors, such as InAs and InSb. The quasi-1d aspect is instrumental for engineering a TSC *without* a Zeeman field [9]. The semiconductor can consist of either two coupled single-channel NWs or a multi-channel film/NW placed on top of a Josephson junction of two conventional SCs. Threading magnetic flux (Φ_{flux}) through the insulating loop (AB Γ Δ) depicted in Fig. 1, can lead to MFs. Apart from using a solenoid, one can generate the required flux via: **i.** a supercurrent flow J_{sc} through the Josephson junction or **ii.** by placing the semiconductor in an electric field \mathcal{E}_{AB} . For the latter two implementations,

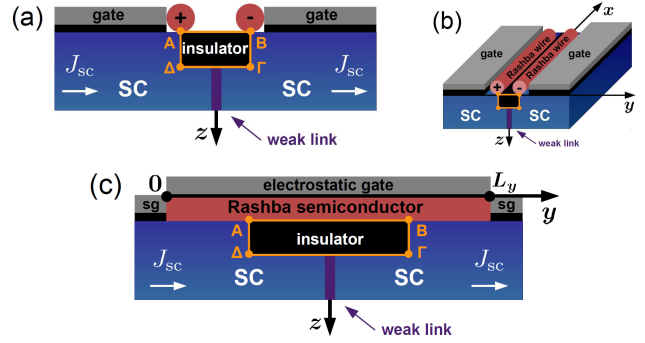


FIG. 1. (a/b) Side/Full view of two Rashba NWs and (c) Side view of a Rashba semiconducting film, on top of a Josephson junction. The interface is interrupted by an insulating loop (AB Γ Δ). Threading magnetic flux (Φ_{flux}) through the loop, leads to Majorana bound states extended along the y axis and localized at the edges along the x axis. The required magnetic flux can be generated by: **i.** a supercurrent flow ($J_{\text{sc}} = 2e\Phi_{\text{flux}}/\hbar$) through the junction or **ii.** by placing the semiconductor in an electric field ($\mathcal{E}_{AB} = \Phi_{\text{flux}}$), produced here by side gates (sg).

the area of the loop can be infinitesimally small. Remarkably, functional devices similar to the one in Fig. 1(c) have been already realized with InAs two-dimensional electron gas (2DEG) [14], rendering the present proposal highly feasible.

The models of the two-NW/channel implementations which I consider here, can be mapped to each other and are characterized by a phase diagram supporting 0, 1 or 2 MFs per edge. The phase with 2MFs per edge is protected by chiral symmetry [5, 15] and meets the zero- and single-MF phases at two quantum tricritical points of the parameter space. By adopting parameter values representative of InAs and InSb, I make firm predictions for experimentally realizing and optimizing the present MF platforms. I find that two coupled NWs can harbor a single MF per edge *only* if they are in contact, while the most promising device relies on a two-channel semiconducting film which supports both 1 and 2 MF-

* panagiotis.kotetes@kit.edu

phases. The latter analysis can be also extended to a three-dimensional Rashba NW in the case where only the lowest three channels become relevant and only two of them can exhibit non-trivial topological behavior. In fact, as I show here, the superconducting proximity effect has to be substantially enhanced for enabling the latter devices to harbor MFs.

For pedagogical reasons, I first present in Sec. II the analysis of a hybrid device relying on two coupled single-channel NWs. In Sec. III I continue with the case of a semiconducting film with only two channels under consideration, which appears as the most experimentally feasible platform of the genre. In Sec. IV, I extend my results to a three-dimensional Rashba NW when only three channels become relevant, and uncover the conditions which can allow the realization of such TSC setups in the lab. Finally, I present my conclusions in Sec. V.

II. TWO COUPLED RASHBA NANOWIRES ON TOP OF A JOSEPHSON JUNCTION

In this section I first introduce (Sec. II A) the accurate three-dimensional Hamiltonian description of the device depicted in Figs. 1(a,b) and highlight (Sec. II B) the intimate connection of threading flux through the loop (AB $\Gamma\Delta$) and imposing a supercurrent flow through the Josephson junction. Later on, I retrieve an effective model for the coupled NWs that incorporates the proximity induced superconducting gap (Sec. II C). For the latter model I perform a symmetry analysis (Sec. II D) which allows uncovering the relevant TSC mechanism (Sec. II E). I conclude this section with extracting the detailed topological phase diagram (Sec. II F) and putting forward concrete predictions for future experiments (Sec. II G).

A. Hybrid-device-Hamiltonian

The model Hamiltonian corresponding to Fig. 1(a) reads: $\mathcal{H} = \int dx [\mathcal{H}_\psi(x) + \mathcal{H}_c(x) + \mathcal{H}_{\psi c}(x)]$ with:

$$\mathcal{H}_\psi(x) = \sum_{n=\pm} \hat{\psi}_n^\dagger(x) [\varepsilon(\hat{p}_x) + v\hat{p}_x\sigma_y] \hat{\psi}_n(x) + [\hat{\psi}_\pm^\dagger(x) (t_\perp + iv_\perp\sigma_x) e^{-i\pi\phi} \hat{\psi}_\mp(x) + \text{H.c.}], \quad (1)$$

$$\mathcal{H}_c(x) = \sum_{n=\pm} \hat{c}_n^\dagger(x) \tilde{\varepsilon}(\hat{p}_x) \hat{c}_n(x) + \tilde{t}_\perp [\hat{c}_\pm^\dagger(x) \hat{c}_\mp(x) + \text{H.c.}] + \sum_{n=\pm} \tilde{\Delta} [e^{niJ_{sc}/2} \hat{c}_{n\uparrow}^\dagger(x) \hat{c}_{n\downarrow}^\dagger(x) + \text{H.c.}], \quad (2)$$

$$\mathcal{H}_{\psi c}(x) = \text{T} \sum_{n=\pm} [\hat{\psi}_n^\dagger(x) \hat{c}_n(x) + \hat{c}_n^\dagger(x) \hat{\psi}_n(x)]. \quad (3)$$

The σ Pauli matrices act on spin space and the operators: $\hat{\psi}_n^\dagger(x) = (\hat{\psi}_{n\uparrow}^\dagger(x), \hat{\psi}_{n\downarrow}^\dagger(x))$ and $\hat{c}_n^\dagger(x) = (\hat{c}_{n\uparrow}^\dagger(x), \hat{c}_{n\downarrow}^\dagger(x))$, create electrons on the NWs and the SCs, respectively. The two parallel *single-channel* NWs ($n = \pm$) are placed

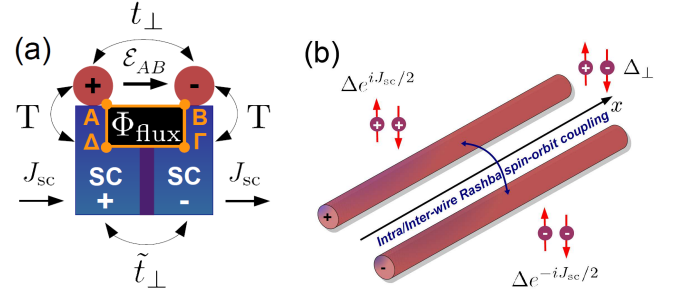


FIG. 2. (a) Cross-section of Fig. 1(b) with couplings: NW-NW (t_\perp), SC-SC (\tilde{t}_\perp), and NW-SC (T). Each cross-section behaves as a superconducting quantum interference device and the total system transits to a TSC phase for a window of values for the inserted flux (Φ_{flux}) in the loop (AB $\Gamma\Delta$). (b) Induced multicomponent superconducting gap on the NWs, when flux is indirectly generated by a supercurrent flow. For $J_{sc} = \pi$, time-reversal symmetry (\mathcal{T}) is violated, since the intra- and inter-NW gaps exhibit a $\pi/2$ -phase locking.

at distance L_y . The terms: $\varepsilon(\hat{p}_x) = \hat{p}_x^2/2m - \mu$, t_\perp , v , v_\perp denote: kinetic energy relative to the chemical potential, inter-NW hopping, intra- and inter-NW SOC. Similarly, $\tilde{\varepsilon}(\hat{p}_x)$ and \tilde{t}_\perp provide the analogous terms for the electrons of the SCs. The above Hamiltonian is obtained for a particular gauge (see App. A), in which the electric field satisfies $\mathcal{E}_{AB} = \dot{\Phi}_{\text{flux}}$ and $\mathcal{E}_{\Delta\Gamma} = 0$. Here $\phi = \Phi_{\text{flux}}/\Phi_0$ denotes the normalized flux ($\Phi_0 = h/2e$). Furthermore, I included the spin singlet superconducting order parameters $\tilde{\Delta} e^{niJ_{sc}/2}$, with a phase difference equal to the supercurrent (J_{sc}) flowing through the Josephson junction. Thus only the gauge invariant quantities, Φ_{flux} and J_{sc} , appear in the Hamiltonian. A cross-section of the heterostructure constitutes a superconducting quantum interference device with the coupled NWs playing the role of the second weak link (Fig. 2(a)), reminiscent of other experimentally realized setups [16].

B. Flux and Supercurrent

Threading flux is usually realized via a solenoid or an electric field given by $\Phi_{\text{flux}} = \int_{t_0}^t dt' \mathcal{E}_{AB}(t')$. The electric induction can be achieved using a capacitor (side gates) which discharges in the presence of an appropriately attached resistive circuit, while $J_{sc} = 0$ is ensured. A discharging event initiated at t_0 yields, in the stationary case of interest, a flux $\Phi_{\text{flux}} = \tau \mathcal{E}_{AB}(t_0)$, with τ the characteristic discharging time. Nonetheless, flux can alternatively arise by inducing a time-independent supercurrent flow equal to $J_{sc} = 2e\Phi_{\text{flux}}/\hbar = 2\pi\phi$ (see App. A), while the electric field is kept zero. Thus, the *simultaneous* control of both quantities is required for engineering a TSC.

C. Effective Hamiltonian

I proceed with integrating out the superconducting degrees of freedom following Ref. [17]. I will consider here a non-zero flux Φ_{flux} , while $J_{\text{sc}} = 0$. To this end, I focus on the last two parts of the complete Hamiltonian, i.e. Eqs. (2) and (3) and transfer to the bonding and anti-bonding basis $\hat{c}_{b,a} = (\hat{c}_+ \pm \hat{c}_-)/\sqrt{2}$, which yields

$$\mathcal{H}_c(x) = \sum_n^{a,b} \left[\hat{c}_n^\dagger \left(\frac{\hat{p}_x^2}{2\tilde{m}} - \tilde{\mu}_n \right) \hat{c}_n + \tilde{\Delta} \left(c_{n\uparrow}^\dagger c_{n\downarrow}^\dagger + \text{H.c.} \right) \right], \quad (4)$$

$$\mathcal{H}_{\psi c}(x) = \text{T} \left(\hat{c}_b^\dagger \frac{\hat{\psi}_+ + \hat{\psi}_-}{\sqrt{2}} + \hat{c}_a^\dagger \frac{\hat{\psi}_+ - \hat{\psi}_-}{\sqrt{2}} + \text{H.c.} \right), \quad (5)$$

with $\tilde{\mu}_b = \tilde{\mu} - \tilde{t}_\perp$ and $\tilde{\mu}_a = \tilde{\mu} + \tilde{t}_\perp$. The latter difference in chemical potentials leads to different density of states at the Fermi level, $\nu_{b,a}$. Moreover, in this new diagonalized basis the bonding and anti-bonding fermions of the superconductor can be integrated out independently, exactly as prescribed in [17]. In the latter works, it has been additionally shown that the corresponding proximity induced gaps, Δ_b and Δ_a , are proportional to the density of states $\nu_{b,a}$. By neglecting for the present discussion the arising renormalization effects [17], we obtain the proximity induced pairing term (also the H.c.) on the NWs

$$\Delta_b \frac{\psi_{+\uparrow}^\dagger + \psi_{-\uparrow}^\dagger}{\sqrt{2}} \frac{\psi_{+\downarrow}^\dagger + \psi_{-\downarrow}^\dagger}{\sqrt{2}} + \Delta_a \frac{\psi_{+\uparrow}^\dagger - \psi_{-\uparrow}^\dagger}{\sqrt{2}} \frac{\psi_{+\downarrow}^\dagger - \psi_{-\downarrow}^\dagger}{\sqrt{2}} \\ = \Delta \sum_{n=\pm} \psi_{n\uparrow}^\dagger \psi_{n\downarrow}^\dagger + \Delta_\perp (\psi_{+\uparrow}^\dagger \psi_{-\downarrow}^\dagger + \psi_{-\uparrow}^\dagger \psi_{+\downarrow}^\dagger) \quad (6)$$

with $\Delta = (\Delta_b + \Delta_a)/2$ and $\Delta_\perp = (\Delta_b - \Delta_a)/2$. By taking into account that $\Delta_{b,a} \propto \nu_{b,a}$, we obtain the relation $\Delta_\perp = \Delta(\nu_b - \nu_a)/(\nu_b + \nu_a)$. Thus, intra- and inter-NW spin singlet superconducting gaps are proximity induced on the NWs, similar to Ref. [7]. The effective Hamiltonian for the NWs, leading to a TSC [9], reads:

$$\hat{\mathcal{H}}_{\text{TSC}}(\hat{p}_x) = \varepsilon(\hat{p}_x)\tau_z + v\hat{p}_x\tau_z\sigma_y - \Delta\tau_y\sigma_y \\ + \left(t_\perp\tau_z\kappa_x - v_\perp\kappa_y\sigma_x \right) e^{i\pi\phi\tau_z\kappa_z} - \Delta_\perp\tau_y\kappa_x\sigma_y, \quad (7)$$

where I employed the spinor $\hat{\Psi}^\dagger(x) = (\psi_{+\uparrow}^\dagger(x), \psi_{+\downarrow}^\dagger(x), \psi_{-\uparrow}^\dagger(x), \psi_{-\downarrow}^\dagger(x), \psi_{+\uparrow}(x), \psi_{+\downarrow}(x), \psi_{-\uparrow}(x), \psi_{-\downarrow}(x))$. The $\boldsymbol{\tau}$ and $\boldsymbol{\kappa}$ Pauli matrices act on Nambu and NW (\pm) spaces. Note that if we would choose to induce the required flux via a supercurrent $J_{\text{sc}} = 2\pi\phi$, we would obtain the equivalent description sketched in Fig. 2(b), with intra-NW gaps $\Delta e^{\pm iJ_{\text{sc}}/2}$ and inter-NW gap Δ_\perp .

D. Symmetry analysis

In the following paragraphs I consider several subcases of the Hamiltonian in Eq. (7), for constant ϕ , with target to provide better understanding of the particular model and reveal the necessary ingredients for engineering time-reversal symmetry (\mathcal{T}) violating TSC phases.

1. $\phi = \Delta_\perp = 0$: No possibility for TSC

In order to expose the topological properties of the Hamiltonian in Eq. (7) and better understand the underlying mechanism for MFs, I first consider $\phi = 0$ and assume, only for demonstration purposes, that I can independently set $\Delta_\perp = 0$ while $\Delta \neq 0$. Under these conditions, the Hamiltonian in Eq. (7) reads:

$$\hat{\mathcal{H}}_{\text{TSC}}(\hat{p}_x) = \varepsilon(\hat{p}_x)\tau_z + v\hat{p}_x\tau_z\sigma_y + t_\perp\tau_z\kappa_x - v_\perp\kappa_y\sigma_x \\ - \Delta\tau_y\sigma_y. \quad (8)$$

For the bulk system, i.e. $\hat{p}_x \rightarrow \hbar k$, the eigenspectrum becomes:

$$E(k) = \pm \sqrt{\Delta^2 + \left[\varepsilon(k) \pm \sqrt{(v\hbar k \pm t_\perp)^2 + v_\perp^2} \right]^2}. \quad (9)$$

By direct inspection we infer that the bulk eigenspectrum cannot support any type of gap closings, therefore no transition is possible from the topologically trivial phase to non-trivial ones, implying that MF-phases are not accessible.

2. $\phi = \pi$ and $\Delta_\perp = 0$: \mathcal{T} -invariant TSC

This situation radically changes if instead $\phi = 1/2$ while $\Delta_\perp = 0$. In this case, the Hamiltonian enjoys the symmetries: $\Theta = \kappa_x\mathcal{K}$ & $\tilde{\Theta} = i\kappa_z\sigma_y\mathcal{K}$ (time-reversal), $\Xi = \tau_x\mathcal{K}$ & $\tilde{\Xi} = \tau_x\kappa_y\sigma_y\mathcal{K}$ (charge-conjugation) and $\Pi = \tau_x\kappa_x$ & $\tilde{\Pi} = \tau_x\kappa_z\sigma_y$ (chiral). Here \mathcal{K} denotes complex conjugation. Note that $\Theta^2 = \Xi^2 = \tilde{\Xi}^2 = +I$ and $\tilde{\Theta}^2 = -I$. Essentially $\tilde{\Theta}$ effects \mathcal{T} , responsible for the emergence of MF Kramers pairs. The two chiral symmetries lead to a unitary symmetry $\mathcal{O} \propto \tilde{\Pi}\tilde{\Pi} = \kappa_y\sigma_y$, which commutes with the Hamiltonian, allowing its diagonalization into two sub-blocks. Via the unitary transformation $\mathcal{U} = (\kappa_z + \kappa_y\sigma_y)/\sqrt{2}$, I diagonalize \mathcal{O} and obtain the two resulting $\kappa = \pm$ sub-blocks:

$$\hat{\mathcal{H}}_\kappa^\mathcal{U}(\hat{p}_x) = \varepsilon(\hat{p}_x)\tau_z + v\hat{p}_x\tau_z\sigma_y + \kappa t_\perp\sigma_y - v_\perp\tau_z\sigma_z \\ - \Delta\tau_y\sigma_y. \quad (10)$$

Each block ($\kappa = \pm$) describes a single channel Rashba NW in the presence of a superconducting gap Δ and a block dependent Zeeman field $\mathcal{B}_\kappa = (0, \kappa t_\perp, -v_\perp)$, with parallel and perpendicular components to the SOC orientation. *In this gauge*, the supercurrent (or flux) converts the inter-NW Rashba SOC into a Zeeman term which is oriented perpendicular to the intra-NW SOC $v\hat{p}_x\tau_z\sigma_y$ [9], as in strictly 1d NW models [3]. Therefore v_\perp is here a *prerequisite* for TSC (this holds also for the general $\phi \neq \pi$ and $\Delta_\perp \neq 0$ case as discussed in App. B). Both blocks belong to symmetry class D, with the charge conjugation symmetry $\Xi = \tau_x\mathcal{K}$. If the value of t_\perp is such, so that the energy spectrum is fully gapped, each subsystem harbors a single MF per edge when $\sqrt{t_\perp^2 + v_\perp^2} > \sqrt{\Delta^2 + \mu^2}$,

associated with the bulk energy spectrum closing at the inversion symmetric point $k = 0$. Due to the underlying \mathcal{T} , the two subsystems transit to the topologically non-trivial phase for the same parameter values, and thus the resulting two MFs per edge constitute a Kramers pair similar to Refs. [6].

However, in contrast to Refs. [6] which focused on \mathcal{T} -preserving TSCs, here I go beyond and study \mathcal{T} -violating TSCs which become accessible after the inclusion of either Δ_\perp or deviations of ϕ from the value $1/2$.

3. $\phi \neq \pi$ and $\Delta_\perp = 0$: Splitting of the MF Kramers pair

Introducing deviations of the flux from the value $\phi = 1/2$, yields the BDI symmetry class with symmetries: $\{\Xi, \Theta, \Pi\}$. It is instructive to study the consequence of small deviations λ , with $\phi = 1/2 + \lambda/\pi$, on the pre-existing MF Kramers pair related to $k = 0$. The Majorana wavefunctions can be retrieved by setting $\hat{p}_x = 0$ in Eq. (10), i.e. $-\mu\tau_z + t_\perp\kappa_z\sigma_y - v_\perp\tau_z\sigma_z - \Delta\tau_y\sigma_y = 0$. By introducing $\tan\delta = \mu/\Delta$ and $\tan\beta = t_\perp/v_\perp$, the MF related eigenvectors have the form $\text{Exp}[-i(\delta\tau_x\sigma_y + \beta\kappa_z\tau_z\sigma_x)/2](1/\sqrt{2})\hat{\mathcal{X}}$ with $\hat{\mathcal{X}}$ (note that *here* the eigenvectors are written for convenience in $\kappa \otimes \tau \otimes \sigma$ space):

$$(0 \ 1 \ 1 \ 0 \ 0 \ 0 \ 0 \ 0)^T, (0 \ 0 \ 0 \ 0 \ 0 \ 1 \ 1 \ 0)^T, \quad (11)$$

$$(1 \ 0 \ 0 \ 1 \ 0 \ 0 \ 0 \ 0)^T, (0 \ 0 \ 0 \ 0 \ 1 \ 0 \ 0 \ 1)^T. \quad (12)$$

The eigenspectrum of the Hamiltonian confined in the above subspace for $\hat{p}_x = 0$, reads:

$$\pm \sqrt{\left(\sqrt{t_\perp^2 + v_\perp^2} - \sqrt{\mu^2 + \Delta^2}\right)^2 + \lambda^2(t_\perp^2 + v_\perp^2)}. \quad (13)$$

For $\lambda = 0$ the eigenenergies touch when $\sqrt{t_\perp^2 + v_\perp^2} = \sqrt{\mu^2 + \Delta^2}$, providing two MF modes. If we switch on λ , no touching can occur and the possibility for zero modes vanishes. Remarkably, one finds that for an arbitrary phase ϕ , the spectrum has always a minimum value, i.e. $|E(k)| \geq \Delta|\cos(\pi\phi)| \forall k$, implying that there can be no gap closing for $\phi \neq 1/2$, as the MFs Kramers pair splits.

4. $\phi = \pi$ and $\Delta_\perp \neq 0$: \mathcal{T} -violating TSC

The situation changes when a non-zero Δ_\perp is added to Eq. (7), not allowing the block diagonalization of the Hamiltonian as in Eq. (10). Instead it yields a single block Hamiltonian residing once again in BDI class with symmetries: $\{\Xi, \Theta, \Pi\}$. By considering a small Δ_\perp , and residing on the analysis of Sec. IID 3 (Eqs. (11),(12)), I find that the modification on the energy spectrum of the preexisting MF Kramers pair of $k = 0$, now becomes:

$$\pm \sqrt{\left(\sqrt{t_\perp^2 + v_\perp^2} - \sqrt{\mu^2 + \Delta^2}\right)^2 + \Delta_\perp^2 \sin^2\beta \sin^2\delta} \\ \pm \Delta_\perp \cos\beta \cos\delta. \quad (14)$$

By inspecting the equation above, it is straightforward to discern that the addition of a small Δ_\perp splits the MF Kramers pair but nevertheless allows for a single touching and thus a single MF mode. Evenmore for large Δ_\perp the system can have the possibility of supporting multiple MFs due to the presence of chiral symmetry in BDI class. In the particular case, one can have up to two MFs per edge, since each MF Kramers pair per edge can still survive in the presence of Δ_\perp , with each one of the previous MF Kramers pair partners now originating from the inversion-symmetry connected points $\pm k_* \neq 0$.

5. $\phi \neq \pi$ and $\Delta_\perp \neq 0$: \mathcal{T} -violating TSC

In the most general case discussed here, MFs are possible due to the presence of Δ_\perp which counterbalances the effect of the deviations of the flux from the value $\phi = 1/2$. Thus, the presence of Δ_\perp is vital for preserving TSC away from $\phi = 1/2$, and can even sustain a pair of MFs per edge in spite of the lifted Kramers degeneracy. In fact, for the parameters considered in the present analysis, Δ_\perp allows the emergence of MFs in the window $0.43 < \phi \leq 1/2$.

E. TSC mechanism

According to the present proposal, crucial ingredient for engineering a \mathcal{T} -violating TSC phase is the combined presence of a supercurrent (or Φ_{flux}) and the inter-NW SC. On one hand, the supercurrent converts the inter-NW SOC into a Zeeman term, while on the other, Δ_\perp guarantees that TSC can survive away from the critical parameter space point $\phi = 1/2$. Notably \mathcal{T} is broken even for $\phi = 1/2$, which constitutes a situation equivalent to inducing a supercurrent flow that realizes a π -junction, depicted in Fig. 2(b). From this point of view, \mathcal{T} -violation can be understood as $\pi/2$ -locking of the multicomponent superconducting gap, since the intra-NW gaps become imaginary ($\pm i\Delta$) and the inter-NW gap remains real (Δ_\perp). Thus the multicomponent superconducting gap violates \mathcal{T} , offering a unique mechanism for obtaining single-MF phases *without* a Zeeman field. Finally, note that a supercurrent flow has been also recently proposed in Ref. [18] as an indispensable ingredient for engineering a TSC, while other works [19, 20] have highlighted its utility for either tailoring [19] or mapping out [20] MF-phases.

F. Topological phase diagram

By virtue of chiral symmetry, I block off-diagonalize the Hamiltonian of Eq. (7) via the transformation $(\tau_z + \tau_x\kappa_x)/\sqrt{2}$. I obtain the k -space Hamiltonian

$$\hat{\mathcal{H}}'(k) = \tau_+ \hat{A}(k) + \tau_- \hat{A}^\dagger(k), \quad (15)$$

with the off-diagonal block projectors $\tau_{\pm} = (\tau_x \pm i\tau_y)/2$ and

$$\hat{A}(k) = \varepsilon(k)\kappa_x + v\hbar k\kappa_x\sigma_y + (v_{\perp}\sigma_x - it_{\perp}\kappa_z)\sin(\pi\phi) + (t_{\perp} + iv_{\perp}\kappa_z\sigma_x)\cos(\pi\phi) - i(\Delta + \Delta_{\perp}\kappa_x)\sigma_y. \quad (16)$$

The relevant \mathbb{Z} topological invariant, \mathcal{N} , is defined as the winding number of $D(k) \equiv \text{Det}[\hat{A}(k)]$ [5]. By employing the unit vector $\hat{g}(k) = (0, D_{\Im}(k)/D(k), D_{\Re}(k)/D(k))$ (see App. C), \mathcal{N} is defined as [18]

$$\mathcal{N} = \frac{1}{2\pi} \int dk \left(\hat{g}(k) \times \frac{\partial \hat{g}(k)}{\partial k} \right)_x. \quad (17)$$

In Fig. 3, I present a series of $v_{\perp} - t_{\perp}$ topological phase diagrams (for further details see App. C), obtained for $\mu = 0$ and representative values for InSb NWs with proximity induced superconductivity, i.e. $v\hbar = 0.20\text{eV}\text{\AA}$, $m = 0.015m_e$ and $\Delta = 250\mu\text{eV}$ [10]. In Fig. 3(a) $\phi = 1/2$ and $\Delta_{\perp} = 90\mu\text{eV}$. Here we find phases with 0, 1 or 2 MFs per edge. The single MF phase is bounded by the lines $\Delta^2 = t_{\perp}^2 + (\Delta_{\perp} \pm v_{\perp})^2$, which are given by the gap closing condition for the inversion-symmetric wavevector $k = 0$ (Fig. 3(c)). On the other hand, the phase with two MFs is associated with gap closings at two non-inversion-symmetric wave-vectors, $\pm k_*$, which are however connected by inversion (Fig. 3(b)). The phase with 2 MFs is topologically protected as long as chiral symmetry $\Pi = \tau_x\kappa_x$ persists [5]. This symmetry could be violated by a mismatch in the intra-NW superconducting gaps (or chemical potentials), which would enter in Eq. (7) with a term $\sim \tau_y\kappa_z\sigma_y$ ($\sim \tau_z\kappa_z$).

For $(\hbar k)^2/2m \gg v\hbar k$, one finds that the gap closings at $\pm k_*$ occur at parts of the parallel lines $t_{\perp} = \sqrt{\Delta^2 - \Delta_{\perp}^2}$ and $t_{\perp} \simeq \Delta$, shown in Fig. 3(a). The phases with $\mathcal{N} = +1$ and $\mathcal{N} = -2$ overlap, leading to the phase with $\mathcal{N} = -1$. As a result, two quantum tricritical points emerge (see also [21]), where the phases with 0, 1 and 2 MFs meet. The latter appear at $P_1 \simeq (\Delta_{\perp}, \Delta)$ and $P_2 = (2\Delta_{\perp}, \sqrt{\Delta^2 - \Delta_{\perp}^2})$. The phase diagram of Fig. 3(d(e)) was retrieved for $\Delta_{\perp} = 50\mu\text{eV}$ and $\phi = 1/2(0.45)$. The tricritical points exist only near $\phi = 1/2$. Evenmore, away from this value the TSC region becomes suppressed. If $t_{\perp} \simeq 0$, the window for a single MF-phase is given by $\Delta - \Delta_{\perp} < v_{\perp} < \Delta + \Delta_{\perp}$. Thus maximizing Δ_{\perp} enhances the robustness of the TSC phase.

G. Predictions for experiments

In reality the two NWs have a finite diameter $d \sim 110\text{nm}$ [10, 22]. If they are in contact, we can assume that t_{\perp} and v_{\perp} are given by the expectation value of the kinetic energy and Rashba SOC component related to hoppings along the y -direction. Therefore, in this case I can set $t_{\perp} = \langle \hat{p}_y^2/2m \rangle \sim \hbar^2/(2mL_y^2)$ and $v_{\perp} = \langle v\hat{p}_y \rangle \sim v\hbar/L_y$, where for a rough estimation I assumed $\langle \hat{p}_y^s \rangle \sim (\hbar/L_y)^s$ with $s = 1, 2$. Under these assumptions, I obtain that for $\phi = 1/2$ and $\Delta_{\perp} = 90(50)\mu\text{eV}$,

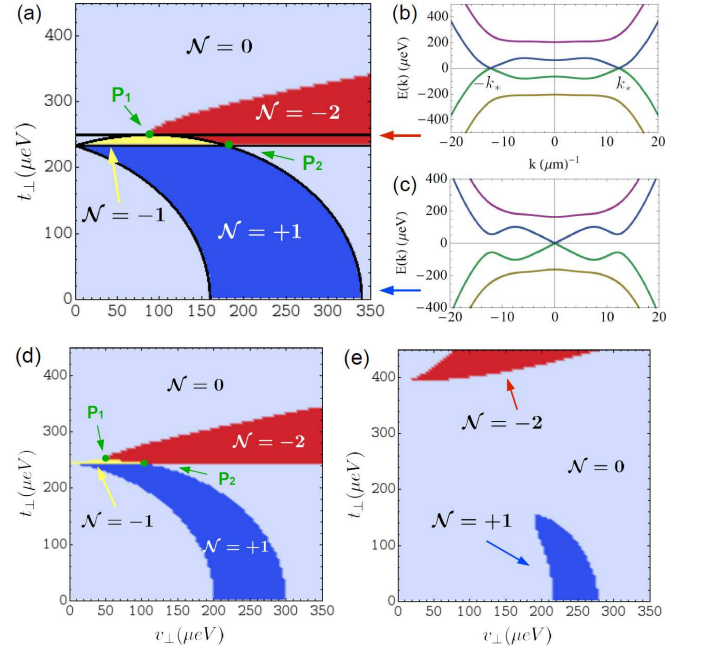


FIG. 3. Topological phase diagrams for InSb and InAs ($\mu = 0$, $\Delta = 250\mu\text{eV}$). (a) $\Delta_{\perp} = 90\mu\text{eV}$ and $\phi = 1/2$ ($J_{sc} = \pi$). Four distinct phases appear: $\mathcal{N} = 0, \pm 1, 2$, with $|\mathcal{N}|$ the number of MFs per edge. The 1MF-phases (blue & yellow) are enclosed by the critical lines $\Delta^2 = t_{\perp}^2 + (\Delta_{\perp} \pm v_{\perp})^2$, defined by the bulk gap closings at $k = 0$, as in (c) for $(v_{\perp}, t_{\perp}) = (300, 136)\mu\text{eV}$. The $\mathcal{N} = -2$ phase is protected by chiral symmetry and arises from gap closings at $\pm k_*$, as in (b) for $(v_{\perp}, t_{\perp}) = (300, 233)\mu\text{eV}$. The $\mathcal{N} = +1$ and $\mathcal{N} = -2$ phases, overlap, yielding the 1MF-phase with $\mathcal{N} = -1$. The latter appears between the parallel lines: $t_{\perp} = \sqrt{\Delta^2 - \Delta_{\perp}^2}$ and $t_{\perp} \simeq \Delta$. Two quantum tricritical points emerge: $P_1 \simeq (\Delta_{\perp}, \Delta)$ and $P_2 = (2\Delta_{\perp}, \sqrt{\Delta^2 - \Delta_{\perp}^2})$, where the 0,1 and 2 MF-phases meet. (d) $\Delta_{\perp} = 50\mu\text{eV}$ and $\phi = 1/2$. Results similar to (a), but with the window for the 1MF-phase suppressed as it depends on Δ_{\perp} . For $\Delta_{\perp} = 0$, the 1MF-phase disappears, since Kramers degeneracy is restored and only MF pairs are allowed. (e) $\Delta_{\perp} = 50\mu\text{eV}$ and $\phi = 0.45$. Further away from the π -junction, the critical points $P_{1,2}$ vanish.

the 1MF-phase can be realized if $105\text{nm} < L_y < 150\text{nm}$ ($110\text{nm} < L_y < 130\text{nm}$). Setting instead $v\hbar = 0.15\text{eV}\text{\AA}$ and $m = 0.024m_e$, addresses the InAs case. By rescaling k , one finds that the topological phase diagrams for InAs almost coincide with those of Fig. 3. For $\phi = 1/2$ and $\Delta_{\perp} = 90(50)\mu\text{eV}$, the 1MF-phase appears in InAs NWs for $80\text{nm} < L_y < 115\text{nm}$ ($85\text{nm} < L_y < 100\text{nm}$). Thus the 1MF-phase is accessible *only* when the NWs are placed *in contact to each other* ($L_y \simeq d$). Otherwise, t_{\perp} and v_{\perp} are associated with electron tunneling and thus become much weaker, as they are given by the exponentially decaying overlap of the NW wavefunctions. Finally, the 2MF-phase appears experimentally inaccessible for the *particular* setup, since it would require for the NWs to be closer than their diameter ($L_y < d$).

III. TWO-CHANNEL RASHBA SEMICONDUCTING FILM ON TOP OF A JOSEPHSON JUNCTION

In the present section I focus on a TSC device consisting of a Rashba semiconducting film (Sec. III A). Its geometry is quasi-1d due to hard-wall confinement along the y axis as in Fig. 4. I consider an effective model constrained to the two lowest confinement channels (Sec. III B). The two-channel model can be mapped to the coupled NW system (Sec. II C), and thus, the symmetry and topological studies of the previous paragraphs (Secs. II D-II F) apply also here. Based on the latter, I predict the design details of such devices for harboring either one or two MFs per edge (Sec. III C).

A. Effective Hamiltonian

The effective Hamiltonian for a Rashba semiconducting film with proximity induced conventional superconductivity, has the form:

$$\mathcal{H} = \int d\mathbf{r} \hat{\psi}^\dagger(\mathbf{r}) \left[\frac{\hat{\pi}^2}{2m} - \mu(t, y) + v(\hat{\pi} \times \boldsymbol{\sigma}) \cdot \hat{z} \right] \hat{\psi}(\mathbf{r}) + \int d\mathbf{r} \Delta(y) \left[\psi_\uparrow^\dagger(\mathbf{r}) \psi_\downarrow^\dagger(\mathbf{r}) + \psi_\downarrow(\mathbf{r}) \psi_\uparrow(\mathbf{r}) \right], \quad (18)$$

where I introduced the gauge invariant canonical momentum

$$\hat{\pi} = \hat{p} + e\mathbf{A} + \hbar\nabla\varphi/2. \quad (19)$$

Here $\mathbf{A} = A_y \hat{y}$ defines the vector potential in the film (equivalent to Φ_{AB} in App. A), while $\varphi = \varphi(t, y)$ is the phase of the bulk SC. Moreover, I introduced the gauge invariant chemical (scalar) potential

$$\mu(t, y) = \mu - \hbar\dot{\varphi}/2 - U_{\text{conf}}(y) + eV_{\text{sg}}(t, y), \quad (20)$$

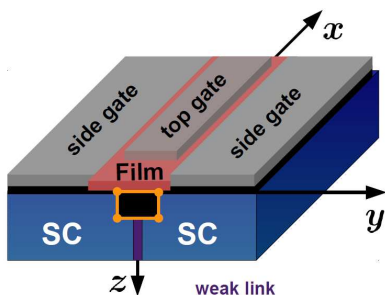


FIG. 4. Full view of a Rashba semiconducting film, on top of a Josephson junction. The interface is interrupted by an insulating loop enclosed by the yellow lines. Threading magnetic flux through the loop, for instance by effecting an electric field using the side gates, leads to Majorana bound states extended along the y axis and localized at the edges along the x axis. The top gate can be employed for tuning the chemical potential of the semiconducting film and thus controlling the topological phase diagram.

consisting of a chemical potential μ , a superconducting phase contribution, a confining potential $U_{\text{conf}}(y)$ and the electrostatic side gate potential $V_{\text{sg}}(t, y)$. Here I consider a confining potential $U_{\text{conf}}(y) = +\infty$ for $y < 0$ and $y > L_y$, and zero otherwise. Its form allows employing the confinement channel wavefunctions $\langle y|n\rangle = \sqrt{2/L_y} \sin(n\pi y/L_y)$ with $n = 1, 2, \dots$ and $\epsilon_n \equiv \langle n|\hat{p}_y^2/2m|n\rangle = (\hbar\pi n)^2/2mL_y^2$. For $v_\perp = 0$ they constitute exact eigenstates of the effective Hamiltonian, while for $v_\perp \neq 0$ they can be employed as a complete basis for furnishing a representation of the latter.

The present effective Hamiltonian has been retrieved by integrating out the superconducting degrees of freedom as in Sec. II C and according to Ref. [17]. Markedly, the superconducting proximity effect is partially blocked, yielding an induced gap $\Delta(y)$ which is zero for $y \in [(L_y - b)/2, (L_y + b)/2]$ and equal to $\bar{\Delta}$ otherwise ($b \equiv (AB)$; see Fig. 1(c)). The particular spatial profile is *required* for retrieving a \mathcal{T} -violating multicomponent gap, similar to Δ and Δ_\perp encountered in the NW case. Instead, if the proximity is not blocked, $\Delta(y) = \Delta$ and no superconducting gap equivalent to Δ_\perp can appear.

By assuming that the vector potential across the interface is zero (equivalent to $\Phi_{A\Delta} = \Phi_{B\Gamma} = 0$ of App. A) and that the spatial dependence of the superconducting phase is of the form $\nabla\varphi = \partial_y\varphi\hat{y}$ we obtain the relation

$$\int_0^{L_y} \left(A_y + \frac{\hbar}{2e} \frac{\partial\varphi}{\partial y} \right) dy = -\Phi_{\text{flux}}. \quad (21)$$

Similarly to the NW case, I set $V_{\text{sg}}(t, y) = \hbar\dot{\varphi}/2e$, and obtain

$$\int_0^{L_y} \mathcal{E}_y dy = \dot{\Phi}_{\text{flux}}. \quad (22)$$

B. Projection onto the two-lowest confinement channels

Since the confinement channel wavefunctions do not constitute eigenstates of Eq. (18), I will consider an approximate model Hamiltonian constructed by the two lowest confinement channels. The validity of the latter Hamiltonian strongly depends on the position of the chemical potential and is expected to break down for large L_y , as in this case the energy level differences become small. Here, I intend to place the chemical potential symmetrically between ϵ_1 and ϵ_2 , i.e. $\mu = 5\epsilon_1/2$, which is achievable with appropriate gating. This value allows focusing on the two-lowest channels, while it additionally constitutes a sweet spot [4], for which charge fluctuations are suppressed.

Care has to be taken, so that the approximate Hamiltonian follows the same gauge transformation rules as the parent Hamiltonian of Eq. (18). In fact, the minimal coupling scheme $\hat{p} \rightarrow \hat{p} + e\mathbf{A}$ must be properly modified. For this reason, I first project the Hamiltonian of Eq. (18) onto the lowest confinement channels,

for $V_{\text{sg}} = A_y = \varphi = 0$. This yields

$$\begin{aligned} \hat{\mathcal{H}}_{\text{film}}(\hat{p}_x) = & \left(\frac{\hat{p}_x^2}{2m} - \mu + \frac{\epsilon_2 + \epsilon_1}{2} \right) \tau_z + v\hat{p}_x\tau_z\sigma_y \\ & + \frac{\epsilon_2 - \epsilon_1}{2} \tau_z\kappa_z - \frac{8v\hbar}{3L_y} \kappa_y\sigma_x \\ & - \frac{\Delta_2 + \Delta_1}{2} \tau_y\sigma_y - \frac{\Delta_2 - \Delta_1}{2} \tau_y\kappa_z\sigma_y, \end{aligned} \quad (23)$$

with the κ Pauli matrices acting on the channel subspace $n = \{2, 1\}$ and $\Delta_n = \int_0^{L_y} dy \langle y|n \rangle^2 \Delta(y)$ given by

$$\Delta_2 = \bar{\Delta} [1 - b/L_y + \sin(\pi b/L_y) \cos(\pi b/L_y)/\pi], \quad (24)$$

$$\Delta_1 = \bar{\Delta} [1 - b/L_y - \sin(\pi b/L_y)/\pi]. \quad (25)$$

In order to introduce the gauge potentials, I will first retrieve the expression for the polarization operator in this basis. The polarization operator reads $P_y = -ey$ and in this basis has the representation $P_y = 16eL_y\tau_z\kappa_x/9\pi^2$. In the presence of a homogeneous time-dependent electric field, \mathcal{E}_y , the Hamiltonian acquires an additional $-P_y\mathcal{E}_y$ term. In the latter case, one can infer the coupling of the two-channel system with the electrostatic potential and the superconducting phase, which reads, $P_y\partial_y(V_{\text{sg}} - \hbar\dot{\varphi}/2e)$. Here I assume that the gradients of the electrostatic potential and superconducting phase are constants. To retrieve the coupling to the vector potential, A_y , we have to first obtain the expression for the paramagnetic current operator $J_y = \dot{P}_y$. The latter time derivative can be retrieved using the Heisenberg equation of motion for the polarization operator calculated using the non-superconducting, and therefore gauge invariant, part of the Hamiltonian in Eq. (23). Thus, we have

$$\begin{aligned} J_y = & \frac{i}{\hbar} \left[\left(\frac{\hat{p}_x^2}{2m} - \mu + \frac{\epsilon_2 + \epsilon_1}{2} \right) \tau_z + v\hat{p}_x\tau_z\sigma_y \right. \\ & \left. + \frac{\epsilon_2 - \epsilon_1}{2} \tau_z\kappa_z - \frac{8v\hbar}{3L_y} \kappa_y\sigma_x, \frac{16eL_y}{9\pi^2} \tau_z\kappa_x \right] \\ = & -\frac{2}{\hbar} \frac{16eL_y}{9\pi^2} \left(\frac{\epsilon_2 - \epsilon_1}{2} \kappa_y + \frac{8v\hbar}{3L_y} \tau_z\kappa_z\sigma_x \right). \end{aligned} \quad (26)$$

The current above provides the linear correction to the Hamiltonian with respect to $A_y + \hbar\partial_y\varphi/2e$. Consequently, the interchannel terms become modified in the following manner

$$\begin{aligned} & \frac{\epsilon_2 - \epsilon_1}{2} \tau_z\kappa_z - \frac{8v\hbar}{3L_y} \kappa_y\sigma_x \rightarrow \\ & \frac{\epsilon_2 - \epsilon_1}{2} \tau_z\kappa_z - \frac{8v\hbar}{3L_y} \kappa_y\sigma_x - J_y(A_y + \hbar\partial_y\varphi/2e) \\ = & \left(\frac{\epsilon_2 - \epsilon_1}{2} \tau_z\kappa_z - \frac{8v\hbar}{3L_y} \kappa_y\sigma_x \right) \times \\ & \left[1 + i\frac{2}{\hbar} \frac{16eL_y}{9\pi^2} \left(A_y + \frac{\hbar}{2e} \frac{\partial\varphi}{\partial y} \right) \tau_z\kappa_x \right]. \end{aligned} \quad (27)$$

The above linear term is useful for calculating the linear response to the external fields, e.g. conductivities, but

can not yield the desired gauge transformation properties. To serve the latter purpose it has to get exponentiated, i.e.

$$\begin{aligned} & \frac{\epsilon_2 - \epsilon_1}{2} \tau_z\kappa_z - \frac{8v\hbar}{3L_y} \kappa_y\sigma_x \rightarrow \\ & \left(\frac{\epsilon_2 - \epsilon_1}{2} \tau_z\kappa_z - \frac{8v\hbar}{3L_y} \kappa_y\sigma_x \right) \text{Exp} \left(-i\frac{32}{9\pi^2} \frac{e\Phi_{\text{flux}}}{\hbar} \tau_z\kappa_x \right), \end{aligned} \quad (28)$$

where I additionally made use of Eq. (21) by considering that A_y is spatially homogeneous. If we now set the total electrostatic potential to zero, i.e. $V_{\text{sg}} - \hbar\dot{\varphi}/2e = 0$, Eq. (21) additionally provides $L_y\mathcal{E}_y = \Phi_{\text{flux}} \Rightarrow \Phi_{\text{flux}} = L_y \int_{t_0}^t dt' \mathcal{E}_y(t')$. Therefore, the normalized flux in the particular case reads $\phi = -(32/9\pi^2)\Phi_{\text{flux}}/\Phi_0$. We immediately notice the difference compared to the NW case, in which $\phi = \Phi_{\text{flux}}/\Phi_0$. The projection onto the lowest two confinement channels yields an effective flux piercing the loop AB Γ Δ , equal to $-32\Phi_{\text{flux}}/9\pi^2 \simeq -0.36\Phi_{\text{flux}}$.

Under the aforementioned conditions and after effecting the unitary transformation $(\kappa_z + \kappa_x)/\sqrt{2}$, the Hamiltonian becomes

$$\begin{aligned} \hat{\mathcal{H}}'_{\text{film}}(\hat{p}_x) = & \left[\frac{\hat{p}_x^2}{2m} - \left(\mu - \frac{5\epsilon_1}{2} \right) \right] \tau_z + v\hat{p}_x\tau_z\sigma_y - \Delta_c\tau_y\sigma_y \\ & + \left(\frac{3\epsilon_1}{2} \tau_z\kappa_x + \frac{8v\hbar}{3L_y} \kappa_y\sigma_x \right) e^{i\pi\phi\tau_z\kappa_z} - \frac{\delta\Delta}{2} \tau_y\kappa_x\sigma_y, \end{aligned} \quad (29)$$

where I introduced the average $\Delta_c = (\Delta_2 + \Delta_1)/2$ and difference $\delta\Delta = \Delta_2 - \Delta_1$ of the superconducting gaps, given by

$$\Delta_c = \bar{\Delta} [1 - b/L_y - \sin(\pi b/L_y) \sin^2(\pi b/2L_y)/\pi], \quad (30)$$

$$\delta\Delta/2 = \bar{\Delta} \sin(\pi b/L_y) \cos^2(\pi b/2L_y)/\pi. \quad (31)$$

Therefore, this Hamiltonian can be mapped to the one of Eq. (7), with the parameters of Eq. (29) having the correspondence:

$$\begin{aligned} \mu & \rightarrow \mu - \frac{5\epsilon_1}{2}, \quad t_{\perp} \rightarrow \frac{3\epsilon_1}{2}, \quad v_{\perp} \rightarrow -\frac{8v\hbar}{3L_y}, \\ \Delta & \rightarrow \Delta_c, \quad \Delta_{\perp} \rightarrow \frac{\delta\Delta}{2}, \quad \phi \rightarrow -\frac{32L_y}{9\pi^2\Phi_0} \int_{t_0}^t dt' \mathcal{E}_y(t'). \end{aligned} \quad (32)$$

As observed in the analysis of the NW case, we can maximize the TSC window via maximizing Δ_{\perp} which here corresponds to $\delta\Delta$. For the two-channel model, this occurs for $b/L_y = 1/3$, yielding $\Delta_c \simeq 3\bar{\Delta}/5$ and $\delta\Delta/2 \simeq \bar{\Delta}/5$. In fact, the latter optimal values will be assumed for the discussion below.

C. Predictions for experiments

The most prominent realization of this setup is based on already existing 2DEG devices [14]. I assume that $\phi = 1/2$, $\mu = 5\epsilon_1/2$, while I set $\bar{\Delta} = 400\mu\text{eV}$, which implies $\Delta_c = 240\mu\text{eV}$ and $\delta\Delta/2 = 80\mu\text{eV}$. Under these conditions, the 1MF-phase is stabilized for InAs when

$315\text{nm} < L_y < 390\text{nm}$. On the other hand, for InSb the 1MF-phase appears for $400\text{nm} < L_y < 500\text{nm}$. In stark contrast to the double-NW case, here the 2MF-phase *becomes* experimentally *accessible*, approximately when: $295\text{nm} < L_y < 310\text{nm}$ for InAs and $370\text{nm} < L_y < 395\text{nm}$ for InSb.

IV. THREE-CHANNEL RASHBA SEMICONDUCTING NANOWIRE ON TOP OF A JOSEPHSON JUNCTION

In this section I consider a hybrid device shown in Fig. 5 in which a three-dimensional Rashba semiconducting NW, confined in the yz plane, lies on top of a Josephson junction (Sec. IV A). For the particular SOC type, the low energy description of the NW requires the consideration of the lowest three-channels (Sec. IV B), on which I focus after having integrated out the superconducting degrees of freedom. According to my analysis, only two of the above three channels become coupled and can in principle exhibit TSC phases, similarly to Sec. III. Using the previous analysis I conclude that the experimental realization (Sec. IV C) of artificial TSC phases in such systems require a quite strong proximity induced gap, which appears not accessible, at least for the moment, using *conventional* SCs, e.g., Al, Nb or Pb.

A. Effective Hamiltonian

In this paragraph I present the effective Hamiltonian for a hybrid device involving a three-dimensional Rashba semiconducting wire. For simplicity, I will here consider a wire with square cross-section $L_y = L_z \equiv d$. The starting point is the Hamiltonian

$$\mathcal{H} = \int d\mathbf{r} \hat{\psi}^\dagger(\mathbf{r}) \left[\frac{\hat{\boldsymbol{\pi}}^2}{2m} - \mu(t, y, z) + v(\hat{\boldsymbol{\pi}} \times \boldsymbol{\sigma}) \cdot \hat{\mathbf{z}} \right] \hat{\psi}(\mathbf{r}) + \int d\mathbf{r} \Delta(y) \left[\psi_\uparrow^\dagger(\mathbf{r})\psi_\downarrow^\dagger(\mathbf{r}) + \psi_\downarrow(\mathbf{r})\psi_\uparrow(\mathbf{r}) \right], \quad (33)$$

with $\hat{\boldsymbol{\pi}} = \hat{\mathbf{p}} + e\mathbf{A} + \hbar\nabla\varphi/2$ and $\mu(y, z) = \mu - \hbar\dot{\varphi}/2 - U_{\text{conf}}(y, z) + eV_{\text{sg}}(t, y)$. Here I assumed that the superconducting gap varies *only* along the y axis, due to the blocked proximity effect by an insulating layer as in the case of the semiconducting film. The consideration of an infinite well confining potential $U_{\text{conf}}(y, z) = 0$ for $\{y, z\} \in \{[0, d], [0, d]\}$ and $+\infty$ otherwise, allows us to introduce the confinement channel wavefunctions $\langle y, z | n, s \rangle = (2/d) \sin(n\pi y/d) \sin(s\pi z/d)$ with $n, s = 1, 2, \dots$ and $\epsilon_{n,s} \equiv \langle n, s | (\hat{p}_y^2 + \hat{p}_z^2) / 2m | n, s \rangle = (\hbar\pi)^2(n^2 + s^2)/2md^2$. The latter constitute eigenstates of the above Hamiltonian for $v_\perp = 0$ while they can be used as a complete basis set for $v_\perp \neq 0$. As in the previous section, I will pursue a low-energy description also here. The energetically lowest level is (1, 1) (corresponding to the set of quantum numbers (n, s)) while the

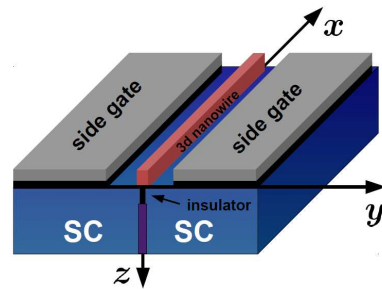


FIG. 5. Full view of a three-dimensional Rashba semiconducting nanowire with square cross-section (yz plane) on top of a Josephson junction. The interface is interrupted by an insulating part (depicted with black) which partially blocks the proximity effect and renders the proximity induced superconductivity inhomogeneous along the y axis. Using the side gates, one can induce an electric field in the semiconductor which in the steady state can support Majorana bound states extended along the y axis and localized at the edges along the x axis.

two energetically higher, (2, 1) and (1, 2), are degenerate. Thus three confinement channels have to be taken into account.

B. Projection onto the three-lowest confinement channels

As in Sec. III B, the projection on the three-lowest channels will be performed first for $A_y = \varphi = V_{\text{sg}} = 0$.

$$\hat{\mathcal{H}}_{\text{wire}}(\hat{p}_x) = \left(\frac{\hat{p}_x^2}{2m} - \mu + \epsilon_1 + \frac{\epsilon_2 + \epsilon_1}{2} \right) \tau_z + v\hat{p}_x \tau_z \sigma_y + \frac{\epsilon_2 - \epsilon_1}{2} \tau_z \begin{pmatrix} 1 & 0 & 0 \\ 0 & 1 & 0 \\ 0 & 0 & -1 \end{pmatrix} - \frac{8v\hbar}{3L_y} \begin{pmatrix} 0 & 0 & 0 \\ 0 & 0 & -i \\ 0 & i & 0 \end{pmatrix} \sigma_x - \frac{\Delta_2 + \Delta_1}{2} \tau_y \sigma_y - \frac{\Delta_2 - \Delta_1}{2} \tau_y \begin{pmatrix} -1 & 0 & 0 \\ 0 & 1 & 0 \\ 0 & 0 & -1 \end{pmatrix} \sigma_y, \quad (34)$$

with the basis $\{(1, 2), (2, 1), (1, 1)\}$. Note that I used $\epsilon_{1,2}$ and $\Delta_{1,2}$ defined in Sec. III A, with $L_y = d$. As seen from the above, in the absence of gauge potentials the channel (1, 2) decouples from the other two. In order to infer if this situation persists for finite gauge potentials, I calculate the polarization operators $P_y = -ey$ and $P_z = -ez$ in this basis. I retrieve

$$P_y = \frac{16ed}{9\pi^2} \begin{pmatrix} 0 & 0 & 0 \\ 0 & 0 & 1 \\ 0 & 1 & 0 \end{pmatrix}, \quad P_z = \frac{16ed}{9\pi^2} \begin{pmatrix} 0 & 0 & 1 \\ 0 & 0 & 0 \\ 1 & 0 & 0 \end{pmatrix}. \quad (35)$$

For the situation considered in this manuscript, the electric field \mathcal{E}_z in the semiconducting wire is zero. Thus for only \mathcal{E}_y finite, the channel (1, 2) decouples even in the presence of gauge potentials and the Hamiltonian for the two remaining coupled channels, (2, 1) and (1, 1), is identical to the two-channel film case of Sec. III A. Note that

the channel (1, 2) can not support MFs. If the proximity induced gap becomes z dependent, then it is possible for the (1, 1) and (1, 2) channels to couple. Nonetheless, even in the latter case the presence of the (1, 2) channel does not change the qualitative topological characteristics and only brings some quantitative modifications to the phase diagram. In order for this channel to become topologically relevant, a different type of SOC has to be considered, which includes also the \hat{p}_z momentum. As a matter of fact, only inter-channel coupling induced by SOC which will be converted into an effective Zeeman term, can lead to new topological properties due to the addition of the (1, 2) channel.

C. Predictions for experiments

By focusing on the two coupled channels, I infer the boundaries for phases with a single MF per edge using the relations $\Delta^2 = t_{\perp}^2 + (\Delta_{\perp} \pm v_{\perp})^2$, as in Sec. II F. For $b = L_y/3$ and a chemical potential symmetrically placed inbetween the levels (2, 1) and (1, 1), as in Sec. III A, I find that the phase with a single MF per edge is realized for a proximity induced gap: $5.2\text{meV} < \bar{\Delta} < 5.8\text{meV}$. Thus it seems *currently* not feasible to engineer a TSC with a single InSb wire, via the proposed mechanism. The reason is the large energy splitting $\sim 3\text{meV}$ of the two coupled channels, compared to the recently experimentally achieved induced superconducting gap using conventional SCs $\sim 0.6\text{meV}$ [22].

V. CONCLUSIONS

To summarize, I proposed a new class of MF platforms relying on low-dimensional semiconductors, which allow

replacing the Zeeman field with supercurrents or electric fields. Double-nanowire setups, which can support 1MF-phases when the nanowires are parallel and in contact to each other, appear experimentally accessible [22]. In contrast, devices based on a three-channel three-dimensional nanowire demand a large proximity induced superconducting gap and can become experimentally feasible if high- T_c superconductors, such as the ones based on Fe [23], can be employed. On the other hand, versatile InAs 2DEG devices in proximity to a Josephson junction which have been already fabricated and manipulated three decades ago, constitute ideal candidates for realizing the two-channel implementation. They can exhibit an interplay of phases with 1 or 2 MFs per edge, depending on the width of the device. Optimization purposes require a supercurrent value of $J_{sc} = \pi$, which can be achieved by connecting the Josephson junction to a large superconducting ring threaded by flux. Alternatively, an electric field $\tau \mathcal{E}_y(t_0) L_y = 9\pi^2 \Phi_0 / 64$ can be applied across the film. For $\tau \sim 1\mu\text{s}$ (ns) and $L_y \sim 400\text{nm}$, a weak field $\sim 70\mu\text{V}(\text{mV})/\text{cm}$ is required, opening new perspectives for *all-electrical* control on MF devices.

ACKNOWLEDGMENTS

I am glad to thank A. Shnirman, G. Schön, A. Geresdi, R. Aguado, V. Mourik, E. Prada, A. Heimes, D. Pikulin, M. Wimmer, J. Schmalian, P.-Q. Jin, D. Mendler and T. Schmidt for valuable discussions and suggestions which significantly helped me to improve and complete this work.

-
- [1] A. Yu. Kitaev, *Annals Phys.* **303**, 2 (2003); C. Nayak, S. H. Simon, A. Stern, M. Freedman, and S. Das Sarma, *Rev. Mod. Phys.* **80**, 1083 (2008); N. Read and D. Green, *Phys. Rev. B* **61**, 10267 (2000); A. Yu. Kitaev, *Phys.-Usp.* **44**, 131 (2001); D. A. Ivanov, *Phys. Rev. Lett.* **86**, 268 (2001); L. Fu and C. L. Kane, *ibid.* **100**, 096407 (2008); J. Alicea, Y. Oreg, G. Refael, F. von Oppen, and M. P. A. Fisher, *Nature Physics* **7** 412 (2011); J. Alicea, *Rep. Prog. Phys.* **75**, 076501 (2012); C. W. J. Beenakker, *Annu. Rev. Con. Mat. Phys.* **4**, 113 (2013).
- [2] J. D. Sau, R. M. Lutchyn, S. Tewari, and S. Das Sarma, *Phys. Rev. Lett.* **104**, 040502 (2010); J. Alicea, *Phys. Rev. B* **81** 125318 (2010).
- [3] R. M. Lutchyn, J. D. Sau and S. Das Sarma, *Phys. Rev. Lett.* **105**, 077001 (2010); Y. Oreg, G. Refael and F. von Oppen, *Phys. Rev. Lett.* **105**, 177002 (2010).
- [4] R. M. Lutchyn, T. Stanescu, S. Das Sarma, *Phys. Rev. Lett.* **106**, 127001 (2011).
- [5] S. Tewari and J. D. Sau, *Phys. Rev. Lett.* **109**, 150408 (2012).
- [6] S. Deng, L. Viola, and G. Ortiz, *Phys. Rev. Lett.* **108**, 036803 (2012); S. Nakosai, Y. Tanaka, and N. Nagaosa, *Phys. Rev. Lett.* **108**, 147003 (2012); A. Keselman, L. Fu, A. Stern, and E. Berg, *Phys. Rev. Lett.* **111**, 116402 (2013); E. Gaidamauskas, J. Paaske, and K. Flensberg, *Phys. Rev. Lett.* **122**, 126402 (2014); A. Haim, A. Keselman, E. Berg, and Y. Oreg, *Phys. Rev. B* **89**, 220504(R) (2014).
- [7] J. Klinovaja and D. Loss, *Phys. Rev. B* **90**, 045118 (2014).
- [8] A. A. Reynoso, and D. Frustaglia, *Phys. Rev. B* **87**, 115420 (2013).
- [9] P. Kotetes, *New J. Phys.* **15**, 105027 (2013).
- [10] V. Mourik, K. Zuo, S. M. Frolov, S. R. Plissard, E. P. A. M. Bakkers, and L. P. Kouwenhoven, *Science* **336**, 1003 (2012).
- [11] M. T. Deng, C. L. Yu, G. Y. Huang, M. Larsson, P. Caroff, and H. Q. Xu, *Nano Lett.* **12**, 6414 (2012); L. P. Rokhinson, Xinyu Liu, and J. K. Furdyna, *ibid.* **8**, 795 (2012); A. Das, Y. Ronen, Y. Most, Y. Oreg, M.

- Heiblum, and Hadas Shtrikman, *ibid.* **8**, 887 (2012).
- [12] E. J. H. Lee, X. Jiang, R. Aguado, G. Katsaros, C. M. Lieber, and S. De Franceschi, Phys. Rev. Lett. **109**, 186802 (2012); A. D. K. Finck, D. J. Van Harlingen, P. K. Mohseni, K. Jung, and X. Li, *ibid.* **110**, 126406 (2013); H. O. H. Churchill, V. Fatemi, K. Grove-Rasmussen, M. T. Deng, P. Caroff, H. Q. Xu, and C. M. Marcus, Phys. Rev. B **87**, 241401(R) (2013); E. J. H. Lee, X. Jiang, M. Houzet, R. Aguado, C. M. Lieber, and S. De Franceschi, Nat. Nanotechnol. **9**, 79 (2014).
- [13] M. Leijnse and K. Flensberg, Phys. Rev. Lett. **107**, 210502 (2011).
- [14] H. Takayanagi and T. Kawakami, Phys. Rev. Lett. **54**, 2449 (1985); M. Thomas, H.-R. Blank, Ki C. Wong, H. Kroemer, and E. Hu, Phys. Rev. B **58**, 11676 (1998).
- [15] R. Wakatsuki, M. Ezawa, Y. Tanaka, and N. Nagaosa, Phys. Rev. B **90**, 014505 (2014); H.-Y. Hui, P. M. R. Brydon, J. D. Sau, S. Tewari, and S. Das Sarma, Sci. Rep. **5**, 8880 (2015).
- [16] J.-P. Cleuziou, W. Wernsdorfer, V. Bouchiat, T. Ondarçuhu, and M. Monthieux, Nat. Nanotechnol. **1**, 53 (2006).
- [17] T. D. Stanescu, J. D. Sau, R. M. Lutchyn, and S. Das Sarma, Phys. Rev. B **81**, 241310(R) (2010); A. C. Potter and P. A. Lee, Phys. Rev. B **83**, 184520 (2011).
- [18] A. Heimes, P. Kotetes, and G. Schön, Phys. Rev. B **90**, 060507(R) (2014).
- [19] B. Seradjeh and E. Grosfeld Phys. Rev. B **83**, 174521 (2011); A. Romito, J. Alicea, G. Refael and F. von Oppen, Phys. Rev. B **85**, 020502 (2012); X.-J. Liu and A. M. Lobos, Phys. Rev. B **87**, 060504 (2013); J. Röntynen and T. Ojanen, Phys. Rev. B **90**, 180503(R) (2014).
- [20] P. San-Jose, E. Prada and R. Aguado, Phys. Rev. Lett. **112**, 137001 (2014).
- [21] R. M. Lutchyn and M. P. A. Fisher, Phys. Rev. B **84**, 214528 (2011).
- [22] S. R. Plissard, I. van Weperen, D. Car, M. A. Verheijen, G. W. G. Immink, J. Kammhuber, L. J. Cornelissen, D. B. Szombati, A. Geresdi, S. M. Frolov, L. P. Kouwenhoven, and E. P. A. M. Bakkers, Nat. Nanotechnol. **8**, 859 (2013).
- [23] Y. Kamihara, T. Watanabe, M. Hirano, and H. Hosono, J. Am. Chem. Soc. **130** 3296 (2008).

Appendix A: Gauge transformation properties of the double nanowire Hamiltonian: Flux & Supercurrent

For clarity, I introduce in this section an extended and more general form of the hybrid device Hamiltonian of Sec. II A:

$$\mathcal{H}_\psi(x) = \sum_{n=\pm} \hat{\psi}_n^\dagger \left[\varepsilon(\hat{p}_x) + v\hat{p}_x\sigma_y - ne\frac{V_{AB}}{2} \right] \hat{\psi}_n + \hat{\psi}_+^\dagger (t_\perp + iv_\perp\sigma_x) e^{i\frac{e}{\hbar}\Phi_{AB}} \hat{\psi}_- + \hat{\psi}_-^\dagger (t_\perp - iv_\perp\sigma_x) e^{-i\frac{e}{\hbar}\Phi_{AB}} \hat{\psi}_+, \quad (\text{A1})$$

$$\mathcal{H}_c(x) = \sum_{n=\pm} \left\{ \hat{c}_n^\dagger \left[\tilde{\varepsilon}(\hat{p}_x) - ne\frac{V_{\Delta\Gamma}}{2} \right] \hat{c}_n + \tilde{\Delta} \left(e^{i\varphi_n} c_{n\uparrow}^\dagger c_{n\downarrow}^\dagger + e^{-i\varphi_n} c_{n\downarrow} c_{n\uparrow} \right) \right\} + \tilde{t}_\perp \left(e^{i\frac{e}{\hbar}\Phi_{\Delta\Gamma}} \hat{c}_+^\dagger \hat{c}_- + e^{-i\frac{e}{\hbar}\Phi_{\Delta\Gamma}} \hat{c}_-^\dagger \hat{c}_+ \right), \quad (\text{A2})$$

$$\mathcal{H}_{\psi c}(x) = \text{T} \left(e^{i\frac{e}{\hbar}\Phi_{A\Delta}} \hat{\psi}_+^\dagger \hat{c}_+ + e^{i\frac{e}{\hbar}\Phi_{B\Gamma}} \hat{\psi}_-^\dagger \hat{c}_- + e^{-i\frac{e}{\hbar}\Phi_{A\Delta}} \hat{c}_+^\dagger \hat{\psi}_+ + e^{-i\frac{e}{\hbar}\Phi_{B\Gamma}} \hat{c}_-^\dagger \hat{\psi}_- \right). \quad (\text{A3})$$

To ensure full generality I have added appropriate voltage drops (V_{ab}) and Peierls'-phases (Φ_{ab}) for all the pairwise coupled elements (a, b) of the hybrid device. For compactness I have suppressed the x dependence of the field operators.

For illustrating the connection between the flux piercing the loop $AB\Gamma\Delta$ and the supercurrent flow, I perform the following gauge transformation $\hat{\psi}_n(x) = e^{nie\chi/2\hbar} \hat{\psi}'_n(x)$ and $\hat{c}_n(x) = e^{nie\alpha/2\hbar} \hat{c}'_n(x)$, with χ and α independent of x . In the new gauge: $V'_{AB} = V_{AB} - \dot{\chi}$, $\Phi'_{AB} = \Phi_{AB} - \chi$, $V'_{\Delta\Gamma} = V_{\Delta\Gamma} - \dot{\alpha}$, $\Phi'_{\Delta\Gamma} = \Phi_{\Delta\Gamma} - \alpha$, $\Phi'_{A\Delta} = \Phi_{A\Delta} - (\chi - \alpha)/2$, $\Phi'_{B\Gamma} = \Phi_{B\Gamma} + (\chi - \alpha)/2$ and $\varphi'_n = \varphi_n - ne\alpha/\hbar$, where \dot{f} denotes the time derivative of f . To this end, I demand: $V'_{AB} = V'_{\Delta\Gamma} = \Phi'_{\Delta\Gamma} = \Phi'_{A\Delta} = \Phi'_{B\Gamma} = 0$, which imposes: $\mathcal{E}_{AB} = \dot{\Phi}_{\text{flux}}$, $\mathcal{E}_{\Delta\Gamma} = 0$, $\Phi'_{AB} = \Phi_{AB} - \chi \equiv -\Phi_{\text{flux}}$, $\varphi'_n = \varphi_n - ne\alpha/\hbar \equiv \varphi_n - ne\Phi_{\Delta\Gamma}/\hbar$, with the electric field $\mathcal{E}_{ab} = V_{ab} - \dot{\Phi}_{ab}$. This additionally provides $\delta\varphi' = \delta\varphi - 2e\Phi_{\Delta\Gamma}/\hbar = J_{\text{sc}}$, i.e., equal to the supercurrent J_{sc} flowing through the junction. Thus only $\Phi'_{AB} \equiv -\Phi_{\text{flux}}$ and $\delta\varphi' \equiv J_{\text{sc}}$, persist in the gauged Hamiltonian, considered also in Sec. II A of the manuscript. For the rest, I will consider that Φ_{flux} and J_{sc} are time-independent. In the steady state, their connection can be demonstrated by performing the additional gauge transformation $\chi \rightarrow \chi - \Phi_{\text{flux}}$ and $\alpha \rightarrow \alpha - \Phi_{\text{flux}}$, yielding $\Phi_{\text{flux}} \rightarrow 0$ and $J_{\text{sc}} \rightarrow J_{\text{sc}} + 2e\Phi_{\text{flux}}/\hbar$. Therefore, threading flux Φ_{flux} is also equivalent to inducing a supercurrent flow $J_{\text{sc}} = 2e\Phi_{\text{flux}}/\hbar$.

Appendix B: Necessary requirement of inter-NW SOC for engineering a TSC

If we set $v_\perp = 0$ in the Hamiltonian of the main text given by Eq. (7), we find that the latter commutes with σ_y and can be diagonalized into two blocks which belong to the AIII symmetry class with the chiral symmetry operator $\tau_x \kappa_x$. By introducing the eigenvectors of σ_y , labelled by $\sigma = \pm 1$, Eq. (16) of the main text can be also block diagonalized with $\hat{A}_\sigma(k) = [\varepsilon(k) + \sigma v\hbar k - i\sigma\Delta_\perp] \kappa_x - it_\perp \sin(\pi\phi) \kappa_z + t_\perp \cos(\pi\phi) - i\sigma\Delta$. Via calculating the winding number of

the unit-vectors $\hat{\mathbf{g}}_\sigma(k) = (0, \text{Det}_{\Im}[\hat{A}_\sigma(k)]/|\text{Det}[\hat{A}_\sigma(k)]|, \text{Det}_{\Re}[\hat{A}_\sigma(k)]/|\text{Det}[\hat{A}_\sigma(k)]|)$, as in Eq. (17), we find that the system always lies in the topologically trivial phase if $v_\perp = 0$.

Appendix C: Topological invariant and bulk gap closings

For $\mu = 0$ and $\phi = 1/2$ one obtains the expressions for the $\mathbf{g}(k)$ vector of Sec. II F:

$$g_y(k) = 4\Delta_\perp v(\hbar k) \left[t_\perp^2 + \Delta_\perp^2 - v_\perp^2 - \Delta^2 - v^2(\hbar k)^2 + \frac{1}{(2m)^2}(\hbar k)^4 \right], \quad (\text{C1})$$

$$g_z(k) = [t_\perp^2 + (\Delta_\perp + v_\perp)^2 - \Delta^2] [t_\perp^2 + (\Delta_\perp - v_\perp)^2 - \Delta^2] + 2v^2(v_\perp^2 - 3\Delta_\perp^2 - t_\perp^2 + \Delta^2)(\hbar k)^2 \\ + \left[v^4 + \frac{2}{(2m)^2}(\Delta^2 + \Delta_\perp^2 - v_\perp^2 - t_\perp^2) \right] (\hbar k)^4 - 2(v/2m)^2(\hbar k)^6 + \frac{1}{(2m)^4}(\hbar k)^8. \quad (\text{C2})$$

The zeroes of $\mathbf{g}(k)$ provide the topological phase boundaries and the bandstructure points where the related gap closing occurs. The gap closings at $k = 0$ give rise to a single MF while the gap closings at $(\hbar k_*)^2/2m = mv^2 \pm \sqrt{(mv^2)^2 + \Delta^2 + v_\perp^2 - \Delta_\perp^2 - t_\perp^2}$ provide two MFs, which are protected by chiral symmetry instead of Kramers degeneracy. The phase with a single MF is enclosed within the area defined by the lines $t_\perp^2 + (\Delta_\perp \pm v_\perp)^2 = \Delta^2$ (dark blue and yellow phase in Fig. 3 of the manuscript), while the phase with two MFs is enclosed within the area defined by the lines $t_\perp = \sqrt{\Delta^2 - \Delta_\perp^2}$, $t_\perp = \sqrt{\Delta^2 - (\Delta_\perp - v_\perp)^2}$ and $t_\perp = \sqrt{\Delta^2 + 2mv^2\sqrt{v_\perp^2 - \Delta_\perp^2}}$ (red phase in Fig. 3 of the manuscript). The phase with the two MFs becomes topologically trivial when chiral symmetry is broken and the system transits to class D, which can happen if an asymmetry between the intra-wire superconducting gaps or chemical potentials is introduced.
